

On the role of topography and wind stress on the stability of the thermohaline circulation

Neil R. Edwards¹, Andrew J. Willmott² and Peter D. Killworth¹

1. *Southampton Oceanography Centre, U.K.*

2. *Keele University, Staffordshire, U.K.*

April 22, 1999

Abstract

A frictional geostrophic model is used to examine how the stability of the thermohaline circulation is affected by idealized topographic variations and the presence or absence of wind stress. If the flow exhibits collapses we consider how topography and wind stress affect the ensuing oscillations. Large scale slope up towards the north or the west can significantly destabilize the circulation by modifying the barotropic flow and reducing the depth of convection. Wind stress stabilizes the circulation by deepening the thermocline in the subtropical gyre. Wind driving can also radically reduce the period of oscillations, by destabilizing the northern halocline in the collapsed phase. The overall period of the oscillation is usually governed by the time taken for diffusive warming to destabilize the deep ocean.

1 Introduction

It has become clear in the last decade that numerical models for the thermohaline circulation using physically meaningful boundary conditions do not always possess steady solutions. The behaviour of the solutions frequently involves an abrupt change known as the polar halocline catastrophe (PHC), which marks the switch between polar sinking, with convection in polar regions, and equatorial sinking with no polar convection. The internal oscillation between these states is observed in two-dimensional (zonally averaged) models (Wright and Stocker 1991), three-dimensional frictional geostrophic models (Winton and Sarachik 1993; Zhang *et al.* 1993) and in the Bryan-Cox primitive equation ocean general circulation model (Bryan 1986).

Oscillations of the thermohaline circulation which involve a PHC have typical periods $O(1000)$ years and can be generated when surface “mixed boundary conditions” are specified. These boundary conditions specify a surface freshwater flux, while the ocean surface temperature is relaxed towards a specified value.

In polar convection regions warm salty water is mixed up to the surface. Consequently there is a rapid loss of heat from the ocean to the atmosphere when surface

mixed boundary conditions are imposed. Over a time scale of order 20 days the ocean to atmosphere heat flux tends to zero (Lenderink and Haarsma 1996; Zhang *et al.* 1993) which helps to stabilise the water column. Stabilisation of the water column is further promoted by the imposed surface freshwater flux and in a PHC high latitude convection is switched off leading to the equatorial sinking “collapsed” state, in which the deep circulation is very weak. Zhang *et al.* (1993) suggest that the damping time scale for sea surface temperature anomalies should be of the order of hundreds of days, which would lead to less temporal variability of the ocean to atmosphere heat flux. This, in turn, would make the PHC of the polar sinking mode of the thermohaline circulation harder to trigger. Zhang *et al.* (1993) also demonstrate that the PHC is less likely to occur if the surface to atmosphere heat flux is held fixed, corresponding to an infinitely long damping time scale. Tziperman *et al.* (1994) show that small changes in surface salinity forcing can destabilize the circulation in a primitive equation ocean model with realistic geometry and forcing. They infer that the large scale circulation of the real ocean may be only marginally stable although, according to Rahmstorf (1996), the representation of convection in particular means that current models may be unable to resolve the issue of the stability of the real ocean.

In a related study of the sensitivity of the thermohaline circulation to surface boundary conditions, Rahmstorf and Willebrand (1995) derive an alternative surface thermal boundary condition. Their boundary condition reflects the fact that large-scale changes in the ocean circulation influence the atmospheric temperature. However, the boundary condition requires the specification of a “climatological” atmospheric equilibrium temperature. Any sea surface temperature anomalies that develop from climatology are weakly damped. Pierce *et al.* (1996) couple an atmospheric energy balance model (EBM) to an ocean general circulation model, thereby removing the need to specify a climatological atmospheric temperature field. The authors find that the thermohaline circulation is more stable than in decoupled ocean circulation studies with mixed boundary conditions.

Shorter, interdecadal period variability of the thermohaline circulation is also well documented (Weaver and Sarachik 1991; Yin and Sarachik 1995) and is usually associated with the location of the convection regions altering in response to the advection of salinity anomalies within the subpolar gyre. The creation and melt of sea ice can also influence the location and strength of convection regions (Zhang *et al.* 1995; Lenderink and Haarsma 1996) and hence play a role in the variability of the thermohaline circulation. Darby and Willmott (1997) demonstrate a new mechanism for generating interdecadal variability of sea ice cover in the Greenland Sea using a coupled EBM, ocean, sea ice model. The mechanism relies upon the impulsive (rapid) weakening of entrainment into the mixed layer at the onset of spring creating an impulsive shoaling of the mixed layer depth which then generates long baroclinic Rossby waves at the eastern boundary. As the waves propagate across the basin an anomalous circulation is established in which cold fresh Arctic water enters the domain interior thereby triggering extra thermodynamic sea ice production. A third type of oscillation, termed a loop oscillation by Winton and Sarachik (1993) and also discussed by Weaver *et al.* (1993) and by Mikolajewicz and Maier-Reimer (1990), is associated with the transport of anomalies by the meridional overturning circulation.

Weaver *et al.* (1993) have performed a thorough investigation of possible influences on the stability and variability of the thermohaline circulation in a primitive equation model in a flat bottom sector domain with mixed boundary conditions. They found that the structure and strength of the surface freshwater flux was the dominant factor controlling stability and variability, with stronger surface freshwater flux leading to increased variability. Winton and Sarachik (1993) found that a double-gyre wind stress can have the opposite effect, tending to stabilize the circulation in a simple domain.

In this paper a frictional geostrophic ocean circulation model, described by Edwards (1996), is used to examine how the stability and period of thermohaline oscillations which have a PHC phase are influenced by (i) topography and (ii) the absence or presence of wind stress. We consider only idealised bottom topography in order to isolate the key physical processes which stabilize the flows. For example a detailed study is carried out for the case in which the topography shallows or deepens in the meridional direction. With topography, the JEBAR term (Slørdal and Weber, 1996) takes the role of a forcing term in the barotropic streamfunction equation. We might anticipate that the location of convection regions will be altered by the presence of topography via the barotropic flow and this, in turn, could influence the stability of the thermohaline circulation. Three possible mechanisms that could alter the stability of the thermohaline circulation with topography are (a) the sloping bottom presenting a physical barrier to the meridional overturning; (b) changes in the circulation arising from the JEBAR term; (c) changes in the intensity and location of convection, perhaps related to (b).

In order to explain changes in the period of the oscillations we revisit the steady, pure diffusion problem considered by Wright and Stocker (1991) and show that our use of a nonlinear equation of state alters their conclusions regarding the existence of steady states; in the nonlinear case steady diffusive solutions can exist which are everywhere statically stable.

The plan of the paper is as follows. Section 2 describes the frictional geostrophic ocean model and the numerical method used for solving the equations. Steady solutions with no topography are discussed in Section 3 and are compared with other, similar published results. A steady solution is examined in Section 4 for the case of a topography which slopes up to the north. The stability of the thermohaline circulation to (i) a slope up to the north; (ii) the absence or presence of wind stress is examined in Section 5. When oscillations which have a PHC phase occur we also examine how (i) and (ii) influence the period. Section 6 addresses the equivalent problem to that in Section 5 but for a downslope to the north. Also in Section 6 we consider the role of the nonlinear equation of state on the steady diffusive solutions of the thermocline equations. Finally, Section 7 summarises the results and outlines future directions for research.

2 Governing equations and numerical method

Our model is based on the thermocline (or planetary geostrophic) equations with the addition of a linear drag term in the horizontal momentum equations. The density depends nonlinearly on the local values of temperature T and salinity S , which obey separate advection-diffusion equations and are also subject to convective adjustment.

Referred to spherical polar coordinates (ϕ, s, z) , where ϕ is longitude, $s = \sin\theta$, θ

is latitude and z is measured vertically upwards, the equations can be expressed in the dimensionless form

$$-sv = -\frac{1}{c} \frac{\partial p}{\partial \phi} - \lambda u + \frac{\partial}{\partial z} \tau^\phi, \quad (1)$$

$$su = -c \frac{\partial p}{\partial s} - \lambda v + \frac{\partial}{\partial z} \tau^s, \quad (2)$$

$$\frac{\partial p}{\partial z} = -\rho, \quad (3)$$

$$\frac{\partial}{\partial \phi} \left(\frac{u}{c} \right) + \frac{\partial}{\partial s} (vc) + \frac{\partial w}{\partial z} = 0, \quad (4)$$

$$\rho = \rho(S, T), \quad (5)$$

$$\frac{D}{Dt} X = \frac{\partial}{\partial \phi} \left(\frac{\kappa_H}{c^2} \frac{\partial X}{\partial \phi} \right) + \frac{\partial}{\partial s} (\kappa_H c^2 \frac{\partial X}{\partial s}) + \kappa_V \frac{\partial^2 X}{\partial z^2} + \mathcal{C}. \quad (6)$$

In the above, $c = \cos \theta$, λ is the drag coefficient and $\boldsymbol{\tau} = (\tau^\phi, \tau^s)$ is the (dimensionless) wind stress. Horizontal lengths have been scaled by the Earth's radius r_0 ; vertical lengths by a typical mid-ocean depth H ; the horizontal velocity components (u, v) in the (ϕ, s) directions have been scaled by a typical horizontal velocity U ; and the vertical velocity w has been scaled by UH/r_0 . The scalings for the perturbation pressure p and density ρ are derived from the geostrophic and hydrostatic relations respectively. Quantity X in (6) represents either temperature T or salinity S and

$$\frac{DX}{Dt} = \frac{\partial X}{\partial t} + \frac{\partial}{\partial \phi} \left(\frac{uX}{c} \right) + \frac{\partial}{\partial s} (vcX) + \frac{\partial}{\partial z} (wX) \quad (7)$$

is the material derivative. Scalings for salt S and temperature T are not necessary because they appear linearly in equation (6); their magnitudes depend on the boundary forcing. The advective time scale r_0/U is used. \mathcal{C} is the convective adjustment term, which acts to remove static instability while conserving S and T . The convection scheme renders each fluid column completely stable at every timestep by iteratively searching for instability and combining adjacent levels into vertically uniform regions. Combining two levels in this way may cause the new region to be unstable with respect to the levels immediately above or below, but since the size of the homogeneous region increases by one vertical level each time instability is detected, it is possible to ensure complete mixing in a small finite number of steps (Rahmstorf 1993). The state equation for the dimensional density ρ_* takes the form

$$\rho_* = 1000 + 0.7968S - 0.0559T - 0.0063T^2 + 3.7315 \times 10^{-5}T^3, \quad (8)$$

which closely approximates the UNESCO formula for observed ocean density in kgm^{-3} if S is in practical salinity units and T in degrees Celsius (Gill 1982). In this and several other respects we follow Winton and Sarachik (1993), who used a similar model to study long period oscillations of the thermohaline circulation which can occur with increased surface salinity forcing.

These equations can satisfy a boundary condition of no normal flow at all boundaries. The no normal flow condition implies a mixed condition on the derivatives of ρ at the

boundary which makes it impractical to specify the gradients of T and S . However, by postulating a distribution of diffusivity κ_H which tends to zero at the lateral boundaries, we can still assume that there is no diffusive flux across these boundaries. Edwards (1996) uses a Frobenius expansion to argue that the resulting mathematical problem is likely to have at least one well-behaved solution near the boundary. Numerical solutions show no sign of instability resulting from this boundary condition. Vertical gradients of T and S are set to zero at the lower boundary while at the upper boundary mixed Dirichlet / Neumann type boundary conditions are used to give the required thermohaline forcing.

The equations are solved in a 60° wide sector of depth H from 10° to 70° North, using surface forcing functions which were found by Winton and Sarachik (1993) to result in a stable steady circulation. Thus the heat flux out of the top grid box is given by

$$-\kappa_V \frac{\partial T}{\partial z} = -\frac{T_a - T_o}{\tau_r} \Delta z, \quad (9)$$

where Δz is the depth of the top grid level, T_o is the temperature in the top grid level, τ_r is a restoring timescale, and the prescribed atmospheric temperature T_a is

$$T_a = A \cos(c_1(\theta - \theta_0)), \quad (10)$$

where A , c_1 and θ_0 are constants. The wind stress at the surface τ_0 is purely zonal with amplitude

$$\tau_0^\phi = B \cos(c_2(\theta - \pi/4)) + C, \quad (11)$$

giving a classical two-gyre pattern, and the surface salinity flux is derived from the gradient of an implied steady state northward flux of salinity F through the basin given by

$$F = \frac{D}{\cos \theta} \sin\left(\frac{\pi(\theta - \theta_0)}{\theta_1 - \theta_0}\right), \quad (12)$$

which implies a surface flux of

$$\frac{3D}{\cos \theta(\theta - \theta_0)} \cos\left(\frac{\pi(\theta - \theta_0)}{\theta_1 - \theta_0}\right). \quad (13)$$

B , C , D , c_2 and θ_1 are constants. Diffusion parameter values have been chosen to ensure numerical stability, while the Rayleigh friction parameter λ in the momentum equation is constrained by the need to have at least one gridpoint in the frictional boundary layers. The values of all the above parameters and their dimensional equivalents, where appropriate, are given in Table 1. Dimensional values have been obtained using a velocity scale $U = 0.05 \text{ ms}^{-1}$ and a depth scale $H = 4000 \text{ m}$, which gives the scale for both barotropic and overturning streamfunctions as 1274 Sv .

To solve the elliptic problem for the barotropic streamfunction we use Gaussian elimination, which is time consuming on the first step but extremely fast thereafter (without topography the equation need only be solved once). The velocities can then be found by an integration in z , and the solution advanced to the next time step, after applying convective adjustment. Spatial gradients, which are second order throughout, are expressed in a difference form such that internal heat and salt fluxes are conserved to numerical accuracy throughout the integration. An explicit first order difference scheme

Table 1: Parameter values, the salt flux equates to a freshwater flux of 1.2 m yr^{-1} at 35 psu at the northern boundary. Dimensional values have been obtained using a velocity scale $U = 0.05 \text{ ms}^{-1}$ and a depth scale $H = 4000 \text{ m}$, which gives the scale for both barotropic and overturning streamfunctions as 1274 Sv .

parameter	value	dimensional equivalent
A	25	25°C
c_1	1.565	–
θ_0	10^0	–
θ_1	70^0	–
B	2.400×10^{-3}	0.07 Nm^{-2}
C	1.029×10^{-3}	0.03 Nm^{-2}
c_2	5.143	–
D	5.064×10^{-3}	$6.452 \times 10^6 \text{ psu m}^3\text{s}^{-1}$
λ	6.349×10^{-2}	$(1.25 \text{ days})^{-1}$
κ_H	0.01	$3185 \text{ m}^2\text{s}^{-1}$
κ_V	1.593×10^{-3}	$2 \times 10^{-4} \text{ m}^2\text{s}^{-1}$
τ_r	4.137×10^{-2}	61 days

is used for timestepping. More than adequate temporal resolution is guaranteed by the small timestep which is necessary to maintain stability. Hence a higher order temporal scheme would be inappropriate. The numerical grid has 20 equally spaced points in each of the s and ϕ directions and 16 logarithmically spaced vertical levels whose separation increases by a factor of ten from top to bottom. To test the model we have repeated the published experiments of Salmon (1990) and Winton and Sarachik (1993) to determine steady states of the system. The results were sufficiently close to validate the model, in spite of differences in the dynamics and numerical methods.

3 Steady solution with no topography

To produce a reference solution the model is integrated in time from a uniform, motionless state for a period of about 2000 years. At this time temperature and salinity are varying only very slowly and we will subsequently refer to this and similar states as steady; unsteady solutions are discussed later. The residual surface heat flux is around $5 \times 10^{-3} \text{ W m}^{-2}$. The final solution is similar to that described in detail by Colin de Verdière (1988,1989); thermal forcing acts to create an anticyclonic gyre at upper levels, which tends to override the wind driving in the north. Strong sinking occurs in the north east corner, where convection is required to balance the heat equation. Away from the northern convection region a thermocline develops with maximum averaged upwelling at about one quarter of the ocean depth. Below the thermocline, advection dominates the budgets of heat and salt except near the northern boundary, and the sense of the

circulation is opposite to that in the upper levels, with a southward flowing western boundary current forming one branch of a cyclonic gyre. These qualitative features are stable to variations of drag and diffusion parameters. With the present values we obtain a maximum in the meridional overturning streamfunction of 21 Sv, and a maximum northward heat flux of 5×10^{15} W. Figure 1 shows temperature and velocity on various horizontal and vertical sections through the model domain.

A useful conceptual picture of this circulation is suggested by Zhang *et al.* (1992) who describe the zonally averaged meridional overturning, which carries the northward heat flux, as only the secondary response to surface thermohaline forcing. Their argument is that if zonally uniform thermal forcing dominates, the resulting geostrophic flow would be eastward at upper levels and westward at depth, from the thermal wind equations. This leads to sinking at the eastern boundary and upwelling of dense fluid at the west. This gives a zonal density variation which drives northward upper level flow and southward flow at depth (again by thermal wind) with northern sinking and southern upwelling. In other words the primary response to surface forcing is a zonal overturning, which distorts isopycnal surfaces in stably stratified regions leading to a secondary overturning in the meridional plane. Combining the zonal and meridional overturning then explains the observed north eastward flow at upper levels.

3.1 Convection and initial conditions

It should be stressed that convection has a very important effect on all these solutions. Without it, the assumption of hydrostatic balance means that there is nothing in our system of equations to prevent solutions from becoming statically unstable. Oceanic convection occurs on scales too small for general circulation models to resolve, and its effects are typically parameterized using functions which are not smooth, posing a significant obstacle to mathematical analysis.

Convection is generally associated with surface buoyancy loss and downwelling. Increasing the strength of the surface forcing in ocean models typically leads to an increase in the size of the convecting region. Colin de Verdière (1988) describes the transition which occurs as the forcing increases from the small amplitude regime, in which the heat balance in the interior is almost totally diffusive, to the fully nonlinear, advection-dominated regime. Convection is almost absent in the linear diffusive regime, but this only occurs for forcing strengths 10 to 100 times less than is considered realistic. Salmon (1990) finds solutions for thermohaline circulations in a simple basin without sacrificing a smooth mathematical representation, by using a prescribed heat source term to represent the effects of convection. Convection has also been parameterized by a local increase of vertical diffusivity (for example Killworth 1989). This is more easily described mathematically but the resulting spatial distribution of diffusivity is likely to be highly complicated.

Surprisingly perhaps, it appears to be possible to find steady solutions without convection. In Zhang *et al.* (1992), such solutions were statically unstable throughout most of the domain, leading to a reversed meridional overturning by the argument given earlier linking the zonal and meridionally averaged cells. We have found slowly varying solutions which are statically unstable only in the north east where convection normally

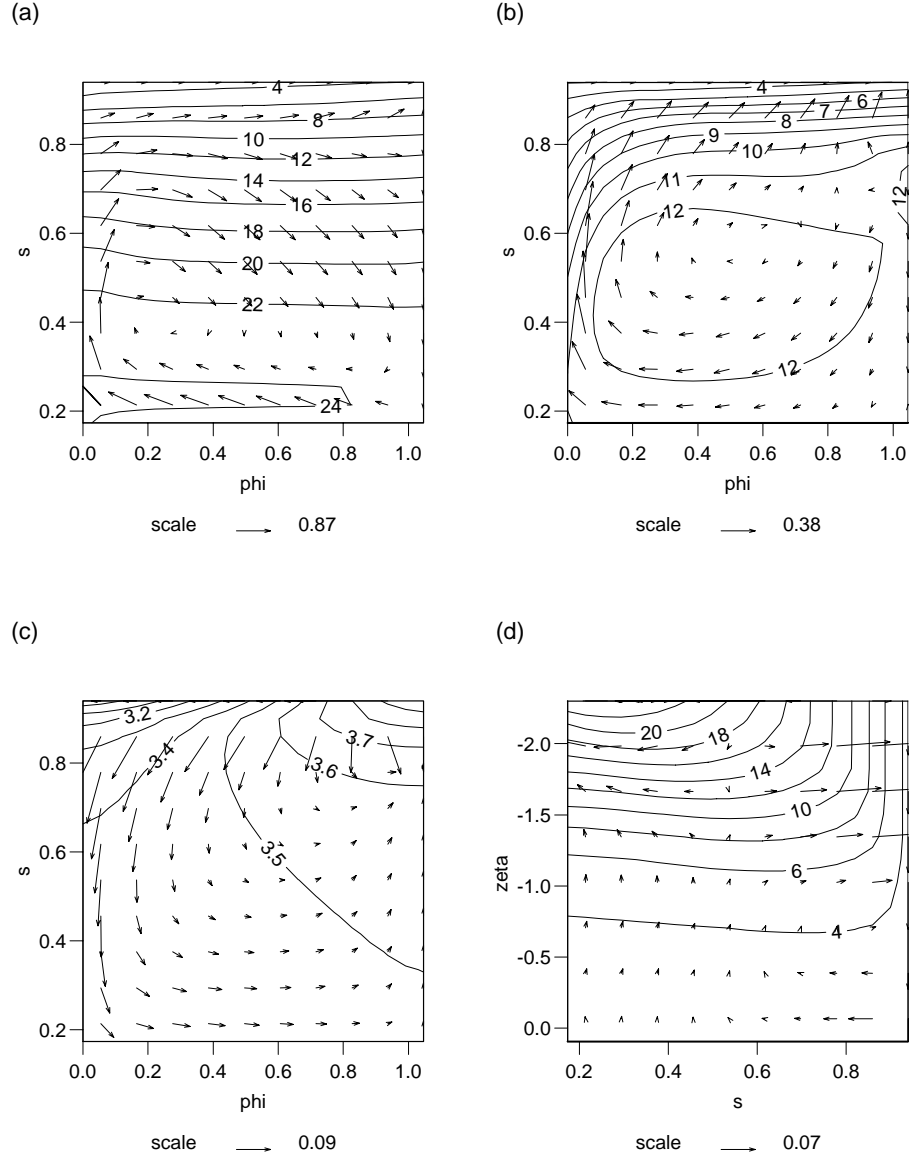


Figure 1: Contours of T and velocity vectors for the standard solution; (a) at the surface $z = 1$, (b) upper thermocline $z = 0.9$, (c) near the bottom $z = 0.1$, (d) vertical meridional section at mid-basin $\phi = \pi/6$. Note that buoyancy driving masks the classical double gyre in the surface velocities. Model vertical levels are uniformly spaced in the logarithmic coordinate $\zeta = \log(1 - z + 0.1)$. Dimensional velocities can be derived by multiplying by $U = 0.05 \text{ ms}^{-1}$. The northward coordinate s is sine latitude.

occurs. The reason for the difference between our solutions and those of Zhang *et al.* (1992) may be the initial condition. In our simulations the ocean initially has a uniform temperature T_0 which lies between the extremal values of the surface forcing temperature. Without convection the temperature in the deep changes only very slowly and even after a thousand years the static stability of the solution is largely determined by the initial condition, if T_0 is small the solution is mostly stable.

The choice of initial temperature T_0 can have a radical effect on the evolution of the solution if convection is included. If T_0 is small the development of the thermal structure is driven by diffusion, and in our simulations the resulting circulation can be dominated initially by the saline forcing. This then leads to a reversed meridional circulation which can persist for thousands of years before a steady thermally dominated state is reached. If T_0 is sufficiently large the temperature structure develops rapidly by convection giving a thermally dominated, northern sinking state. In every case studied we have found that if T_0 is set to the largest value of T_a , then either (i) the solution converges essentially monotonically towards a thermally dominated steady state or (ii) the solution oscillates and no steady state is found.

If the system has multiple steady states for given forcing, choosing a large value of T_0 might be expected to favour a steady state with thermally dominated overturning and convection. Rahmstorf (1995) found that multiple steady states could exist in an ocean general circulation model (OGCM) which were characterized by different patterns of convection. Lenderinck and Haarsma (1994) describe how even a three point “box” model can have solutions with or without convection. The box model results suggest that certain grid points in numerical model solutions could be in a convecting or non-convecting state with only minor alterations to the rest of the solution. They test this hypothesis using a three-layer numerical model solution and find that the model can be perturbed from one steady state into another. In our model changes in T_0 did not result in different steady states. A limited investigation of localised initial salinity perturbations produced only one case (with low vertical resolution in the thermocline and a steeply sloping bottom) where two steady solutions existed for the same forcing. Note that with fixed surface salinity flux the absolute value of salinity has no dynamical effect since our equation of state is linear in salinity. Coarse resolution and relatively high values of diffusion probably reduce the potential for multiple solutions.

3.2 Mixed boundary conditions

The contrasting surface feedbacks on temperature and salinity in the ocean lead to a number of important effects which are most clearly demonstrated using so called “mixed” Dirichlet / Neumann boundary conditions. Using mixed boundary conditions probably overestimates these effects, but is in keeping with our aim of using relatively simple models to improve qualitative understanding.

The heat flux boundary condition, which is mathematically equivalent to fixing the temperature at a point above the surface, allows the surface heat flux to respond to changes in surface temperature. This can lead to a positive feedback on the strength of convection; surface heat loss contributes to surface cooling which can cause convection, this is likely to bring up heat from below which further increases the rate of heat loss

at the surface. This process is probably very important in reinforcing the strength of the thermally driven overturning circulation. With mixed boundary conditions no such feedback operates in regions where convection is driven by the constant surface salinity forcing. Hence the reversed saline driven circulations are weaker and in our simulations always ultimately collapse.

4 Solutions with bottom topography

4.1 Conditions

We now consider the effect of simple variations in bottom topography on the basic solutions described in Section 3. As before the domain is a 60° wide sector extending from 10° to 70° North. The topographic variation will be either a shallowing towards the pole (upslope); a deepening towards the pole (downslope); or a shallowing towards either the eastern or western boundary. Topography is represented as a series of steps. The upslope is designed to represent in a crude and qualitative way the northward decrease in average depth of the North Atlantic. The downslope runs are principally intended to complement the upslope runs for the purpose of improving understanding of the relevant fluid dynamical processes at work, and can be taken to represent generically the effects of large-scale slopes downwards towards the pole. The runs with bottom slope to the east or west are also intended to model generic processes rather than specific oceanographic locations, and are discussed only briefly. For the upslope runs, the computational domain is constrained vertically to the region; $\max(1, 1 + n(j - 16)) \leq k \leq 16$ for $j = 1, \dots, 20$, where j indexes the northward coordinate $s = \sin(\text{latitude})$ and k indexes the stretched vertical coordinate $\zeta = \log(1 - z + 0.1)$ and the slope parameter $n = 1, 2$ or 3 . Fig. 2 shows a cross-section of the grid for slope parameter $+2$, and for the downslope geometry defined below. Stretching of the grid in both horizontal and vertical directions results in a bottom slope whose gradient decreases towards the north. The eastern and western slopes are defined in an exactly analogous way.

For the downslope run it was desirable to maintain the same distribution of vertical levels, particularly throughout the thermocline region, in order to enable meaningful comparisons to be made with the other runs. The chosen form of the downslope is essentially a reflection of the upslope; that is, if the the height of the topography above a basic depth is given by $h(s)$ in the upslope run, then the corresponding height in the downslope run is given by $-h(s)$. For numerical reasons however, this holds only up to a certain latitude whereafter the depth remains constant. This is because a trench is created which must be at least 3 gridpoints wide to be resolvable by the present numerical code. A slope parameter of $+2$ corresponds to a decrease in bottom depth from 4 km to 1 km between 52° and 70° North, or an average gradient of 1.5×10^{-3} . The runs to be described below are each defined by a label of the form SnWRm, where n is the integer slope parameter described above, negative n corresponding to downslope; the presence or absence of the letter W indicates the presence or absence of wind forcing; and m is a constant factor which multiplies the surface evaporation-precipitation (rain) flux. Unless otherwise stated, all other parameters are the same as used in the basic solution described earlier, thus the basic solution has the label S0WR1.

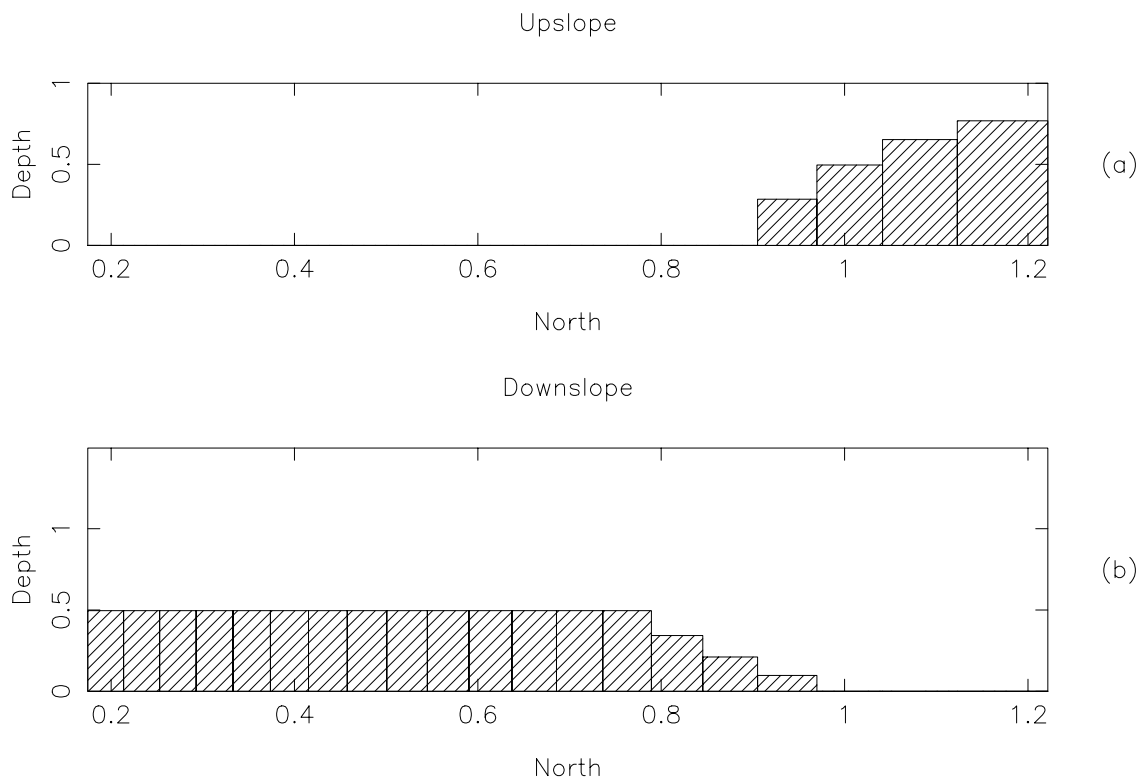


Figure 2: North-south cross-section of the model grid for slope parameter +2 (a), and -1 (b). The latitude, given in radians, ranges from 10^0 to 70^0 North. The dimensionless depth in the southern part of the domain is 1 for all values of slope.

4.2 Topographic forcing

Variations in bottom topography can drive barotropic flows if the fluid density varies along the slope, that is if isopycnals above the slope are not parallel to isobaths. This topographic forcing, sometimes referred to as the joint effect of baroclinicity and relief (JEBAR), is associated with a term in the equation for the barotropic streamfunction Ψ . The barotropic velocity \mathbf{u}^+ is related to Ψ according to

$$H\mathbf{u}^+ = \int_{-H}^0 \mathbf{u} dz = \mathbf{k} \times \nabla \Psi, \quad (14)$$

where H is the ocean depth and the surface is at $z = 0$. Ψ obeys the equation

$$J(\Psi, \frac{s}{H}) + J(E, \frac{1}{H}) + \nabla \cdot (\frac{\lambda}{H} \nabla \Psi) - \mathbf{k} \cdot \nabla \times (\frac{\boldsymbol{\tau}_0}{H}) = 0, \quad (15)$$

where

$$E = \int_{-H}^0 z \rho dz. \quad (16)$$

$J(A, B)$ is the Jacobian $A_\phi B_s - A_s B_\phi$. Without topography, wind forcing (the last term in 15) is balanced by planetary vorticity advection (the first term), with a boundary current at the west in which the term in λ representing frictional drag also becomes important. The second term in (15) represents forcing by JEBAR.

4.3 Results

Figure 3 shows that the effect of upslope on Ψ in run S2WR1 is to reinforce the wind-driven subpolar gyre. The minimum value of Ψ in run S2WR1 is -2×10^{-2} (25 Sv), as compared to -3×10^{-3} (4 Sv) for the flat bottomed standard run (S0WR1). Upslope also causes the gyre centre to shift to the western boundary. In thermally dominated solutions of our model such as the standard solution, isopycnals tilt downwards to the east in the subpolar region. The gradient of E therefore points to the west so that with depth decreasing northwards the JEBAR term is negative over the slope; the same sign as the wind stress term in this region. In run S2WR1 the average value of the JEBAR term over the slope is -0.3 while in the flat bottomed run S0WR1 the average value of the wind forcing term is -0.01. Hence there is a much stronger subpolar gyre in the run with topography.

Figure 4 shows temperature and velocity fields analogous to figure 1. Away from the slope region the solutions are similar, but the deep is warmer and more isothermal with slope, while the northern wall is slightly cooler. In the next section we address the dynamical consequences of the slope for the nature of oscillations supported by the model.

5 Deep decoupling oscillations

With sufficiently strong surface salinity forcing the thermally driven overturning circulation in our model collapses to a weaker, surface-trapped circulation with sinking in the

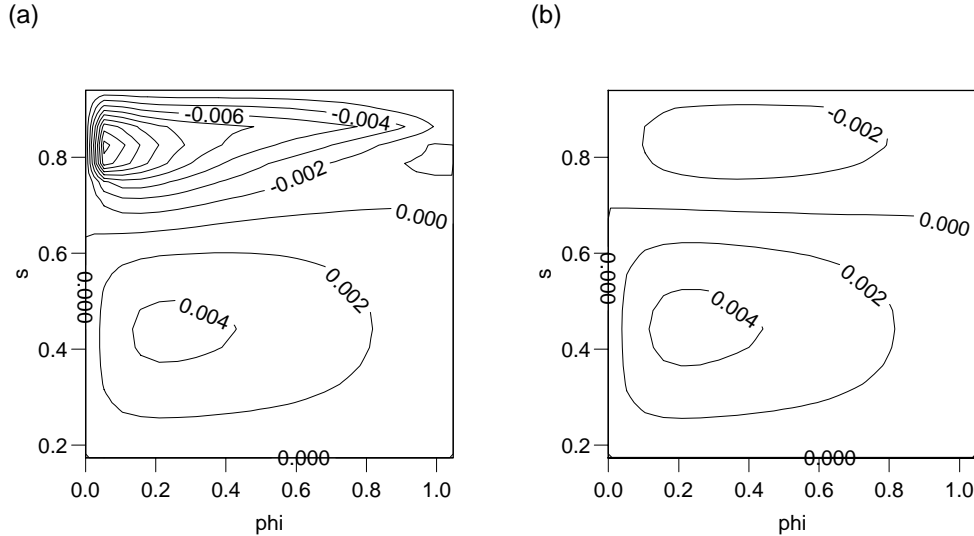


Figure 3: The barotropic streamfunction for runs S2WR1 (a) and S0WR1 (b). Dimensional values can be derived by multiplying by 1274 Sv. The northward coordinate s is sine latitude.

south and upwelling in the north. This collapsed mode is unsteady and an oscillation results which typically has a period of several thousand years. The deep water progressively warms during the collapsed phase until a large region of fluid becomes statically unstable. This results in a powerful “flush” in which northern convection releases the heat accumulated by the deep water. During the flushing phase the circulation pattern, which resembles the thermally dominant steady states, becomes weaker with time and finally collapses again, completing the cycle. Figure 5 shows the variation of the average temperature in the deep during runs S0WR2.7, S2WR2.7 and S0R2.7 (unless otherwise stated the term “deep” refers to the lower half of the computational domain, which roughly corresponds to the region below the thermocline).

A dramatic collapse of the thermally driven overturning was first found by Bryan (1986) who described how strong salinity forcing creates a freshwater pool in the north which shuts off the northern convection resulting in the what he termed a polar halocline catastrophe. The ensuing oscillations were investigated by Wright and Stocker (1991) in the context of a zonally averaged model, and by Weaver *et al.* (1993) in a primitive equation model. In this study we use the same surface forcing functions as Winton and Sarachik (1993) who found these oscillations, which they termed “deep decoupling oscillations”, in both two and three-dimensional versions of a planetary geostrophic model similar to ours.

In this section we consider how topography and also wind stress affect the stability of our model to these deep decoupling oscillations. The strength of salinity forcing has been varied (by a constant factor) to approximately locate the minimum forcing amplitude required to give oscillations. This minimum represents a stability boundary, the location of which will vary with bottom slope and wind stress. We also discuss how

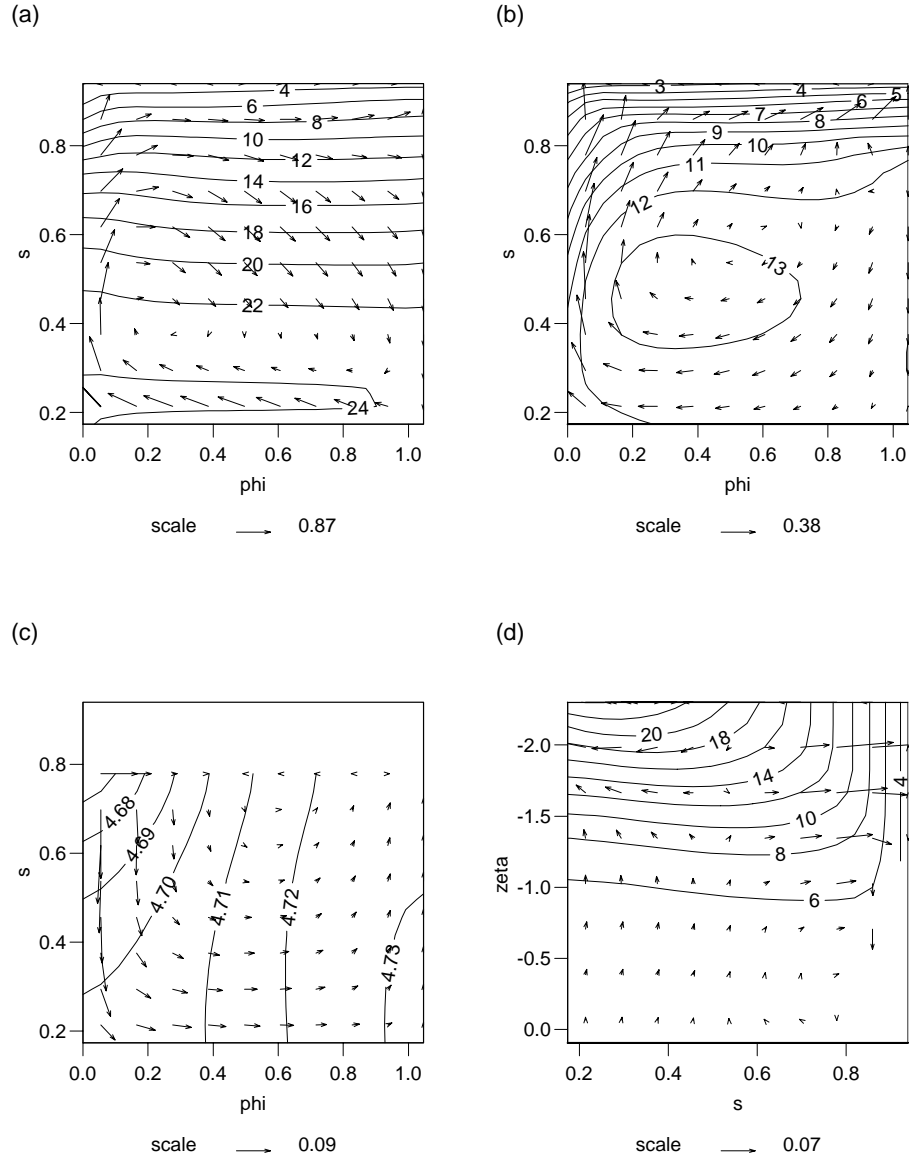


Figure 4: Contours of T and velocity vectors for run S2WR1 with reduced depth in the north; (a) at the surface $z = 1$, (b) upper thermocline $z = 0.9$, (c) near the bottom $z = 0.1$, (d) vertical meridional section at mid-basin $\phi = \pi/6$. Model vertical levels are uniformly spaced in the logarithmic coordinate $\zeta = \log(1 - z + 0.1)$. Dimensional velocities can be derived by multiplying by $U = 0.05 \text{ ms}^{-1}$. The northward coordinate s is sine latitude.

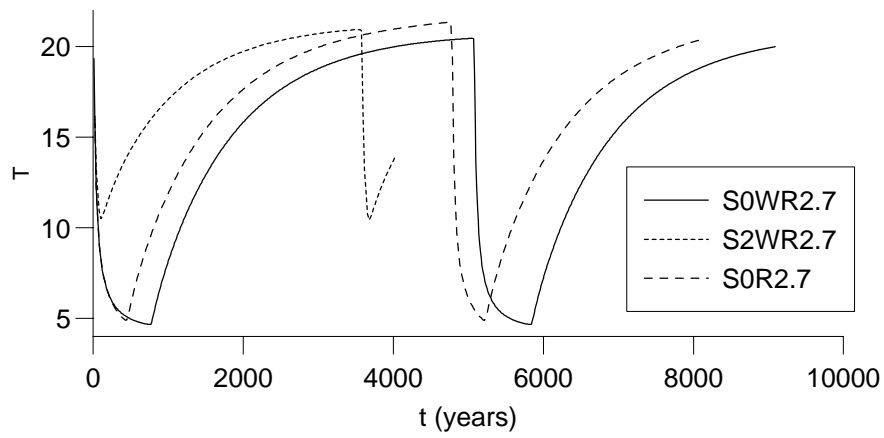


Figure 5: Average deep temperature for runs S0WR2.7 with wind, S2WR2.7 with wind and slope up to the north, and S0R2.7 with no wind.

slope, wind stress and salinity forcing affect the period of the oscillations.

5.1 Effect of bottom slope on the stability boundary for oscillations

To find the stability boundary we ran the model several times starting from an initial condition of uniform salinity, with the temperature everywhere set equal to the largest value of the surface forcing temperature T_a . As discussed in Section 3.1 our experience suggests that this initial condition favours a thermally driven state and will result in essentially monotonic convergence towards such a state if one exists for the forcing level imposed. The model is integrated in each case for the same period of around a thousand years (strictly to $t = 250$ or 1010 years), during which time the circulation slows down and the basin cools. Above a certain amplitude of forcing the flow collapses before the end of the run. Therefore the bifurcation point which we define in this way is actually an approximate minimum forcing amplitude required for the solution to collapse in less than a thousand years.

As the forcing is reduced towards the approximate bifurcation point the time taken for the thermally driven overturning to collapse increases rapidly, while for weaker forcing the solutions appear to be approaching an exactly steady numerical state. Therefore it seems likely that there is a true bifurcation between steady and unsteady model solutions close to the value we find. If the flow has not collapsed before a thousand years it is changing only very slowly at this time; the average surface heat loss is typically around 0.05 W m^{-2} . In one case a marginally stable run was integrated a further thousand years without collapsing. Solutions discussed later with no advection or convection were found to converge exactly.

Figure 6 shows the variation of the approximate bifurcation point with slope, with and without wind forcing. For flat-bottomed, wind-forced runs the bifurcation from steady solutions (as defined above) to oscillating solutions occurred between runs S0WR2.6 and S0WR2.7, that is for a relative salinity forcing amplitude of around 2.7. With slope amplitude 2 the bifurcation occurred at around 1.7. The presence of an upward sloping bottom therefore significantly reduces the stability of the solution to deep decoupling oscillations.

The destabilizing effect of the upslope is related to a reduction in the thermally induced meridional overturning Ψ_M . The maximum value of Ψ_M is 1.65×10^{-2} (equivalent to 21 Sv) for the steady run S0WR1 but the addition of slope in the steady run S2WR1 results in a maximum value of Ψ_M of only 1.25×10^{-2} (16 Sv). Three effects can be identified which contribute to this reduction in overturning: firstly the slope may physically obstruct the overturning; secondly there are destabilizing effects caused by JEBAR; thirdly with reduced depth in the north, convection in the northern sinking region cannot reach the deepest water in the basin. We consider each of these effects in turn to assess their relative importance.

Firstly, to attempt to isolate effects which depend only on domain shape, we have run the model with and without bottom slope, but with no convection and no barotropic flow. Turning off the barotropic flow when there is topographic variation is a useful but unphysical device. Imposing a barotropic flow which is not the solution of (15) implies

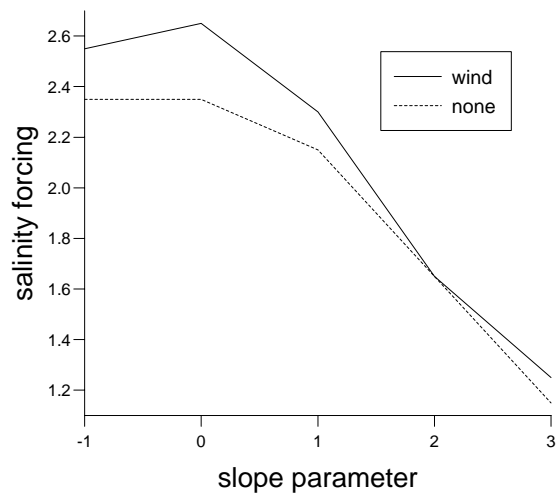


Figure 6: Relative strength of salinity forcing found to result in a transition between steady and oscillating solutions with a sloping bottom in the north. The gradient of the slope increases with slope parameter, and the bottom is flat for slope parameter equal to zero.

that the momentum equations are not satisfied at every level, although the interior dynamics remain true to the thermal wind relations. Also the sinking is less deep without convection, so the effect of the slope is reduced. Differences between the two runs will be affected by the step-like discretization of the slope, which is therefore to some extent a numerical artifact of this type of grid related to the problems with horizontal boundaries discussed by Marshall (1996), and further complicated by the differences between the horizontal and vertical momentum balances (see also Adcroft *et al.* 1996). Fortunately, from the point of view of interpretation, the difference in maximum overturning between the two runs is small. Without slope, wind, salinity forcing or convection the maximum of Ψ_M at 1000 years is 9.12×10^{-3} . In the equivalent run with slope but no barotropic flow the maximum value of Ψ_M at 1000 years is 9.09×10^{-3} .

We turn now to the effect of JEBAR on Ψ_M . JEBAR forcing creates a strong westward flow in the north of the domain which diverts the strongly sinking fluid. This effect is clearly evident in the meridionally averaged zonal overturning streamfunction Ψ_Z for the steady run S2WR1 which has a two-cell structure with sinking only to intermediate depth at the eastern boundary. This contrasts with the single cell structure of Ψ_Z in run S0WR1 with deep sinking at the east, contours of Ψ_Z for both runs are shown in figure 7. The maximum value of Ψ_Z in run S2WR1 is only 9×10^{-3} as compared to 1.8×10^{-2} in run S0WR1. If we view the meridional overturning as a result of distortion of isopycnal surfaces by the zonal overturning, then a reduction in Ψ_Z should lead to a reduction in Ψ_M . To attempt to assess the importance of this effect we have run the model to a steady state, firstly with the barotropic flow artificially set to zero with slope +2, and also with the barotropic streamfunction from the end of the sloping bottom run S2WR1 artificially imposed on the flat bottom run S0WR1. The results of these runs on the maximum value of Ψ_M were as follows (recall that the maximum value of Ψ_M in run S0WR1 is 1.65×10^{-2} and in run S2WR1 1.25×10^{-2}). Artificially removing JEBAR gave a maximum of 1.58×10^{-2} , while artificially adding JEBAR to a flat run gave a maximum of 1.54×10^{-2} . The two experiments demonstrate that the topographically forced barotropic flow acts strongly to reduce Ψ_M , but that other effects must also be important.

Finally we contrived to investigate how the obstruction to deep convection affects the overturning by running the model to a steady state with a flat bottom, but with convection only in the region above an imaginary surface of slope +2. In spite of the unorthodox conditions the solution converged to a steady state, with only a small amount of noise restricted to the northern boundary. The pattern of meridional overturning was similar to the flat bottomed case showing that although convection strongly favours deep sinking, the model does not need to convect to the deepest water in the far north to maintain deep sinking there. The maximum value of Ψ_M for this run was 1.26×10^{-2} , indicating that changes in convection, possibly linked to topographic forcing of the flow, may account for most of the reduction in overturning.

In summary, convection and topographic forcing interact strongly and nonlinearly, but the results suggest that the westward diversion of sinking fluid and the reduced depth of convection both contribute significantly to the destabilization of the flow.

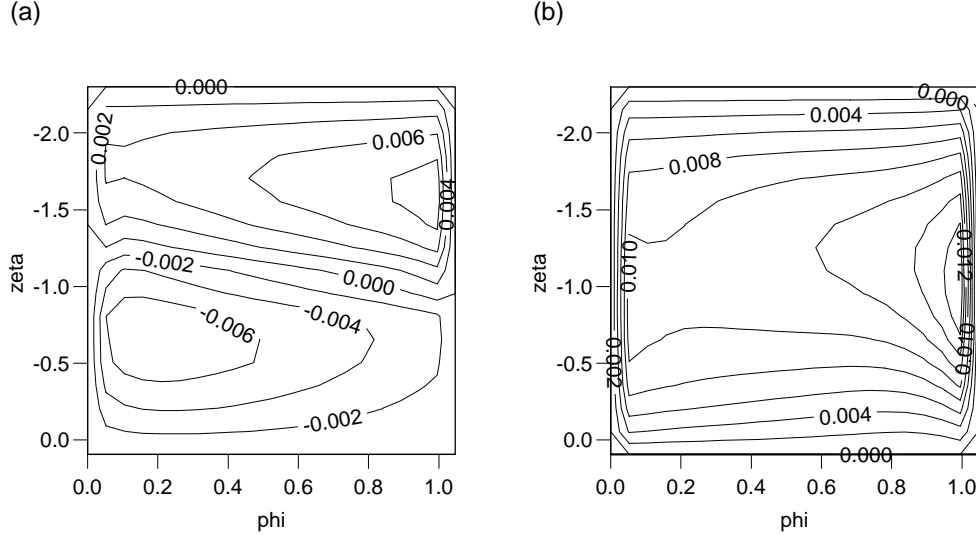


Figure 7: Meridionally averaged zonal overturning streamfunction for runs S2WR1, with slope up to the north (a) and S0WR1, with a flat bottom (b). Dimensional values can be obtained by multiplying by 1274 Sv.

5.2 Effect of wind on the stability boundary for oscillations

Wind stress results in stronger meridional overturning in steady solutions and a related increase in the stability of solutions to the onset of deep decoupling oscillations. Without wind stress the bifurcation to oscillations is found to be between runs S0R2.3 and S0R2.4 (Recall that with wind the bifurcation occurred between runs S0WR2.6 and S0WR2.7). However with slope parameter +2 the presence or absence of wind stress did not affect the stability boundary to within a salinity forcing factor of ± 0.05 (Figure 6). The bifurcation occurred for a salinity forcing amplitude between 1.6 and 1.7 in either case.

Why should steady states with the wind stress (11) have more overturning, when the initial effect of adding wind stress is to decrease the overturning? The reason is that the wind stress increases the depth of the thermocline as noted by Zhang *et al.* (1992). To demonstrate this we examine two runs, one with and one without wind stress; S0WR0 and S0R0. The salinity forcing was set to zero for clarity. Wind stress appears as an extra term in the momentum equations in the mixed layer. This also leads to a wind stress term in the equation for the barotropic streamfunction. Linearity in these equations means that we can write the velocity field as the sum of a velocity field \mathbf{u}_w which results directly from these forcing terms, plus a thermohaline component driven by the density variations. \mathbf{u}_w is constant in time in our model, and we can consider the difference $\mathbf{u}_1 - \mathbf{u}_2$ between the velocity fields in the steady solutions with and without wind, to be the sum of this directly wind-forced velocity plus some residual difference resulting from density variations induced by the wind stress; $\mathbf{u}_1 - \mathbf{u}_2 = \mathbf{u}_w + \mathbf{u}_{wi}$. It turns out that \mathbf{u}_{wi} overrides \mathbf{u}_w throughout much of the domain. Figure 8 shows the zonal averages of \mathbf{u}_w , \mathbf{u}_{wi} , and the velocity fields from the two steady states. The directly

wind-forced overturning pattern for the double gyre wind stress consists of two cells which meet in a downwelling region at the Ekman convergence zone in mid-latitudes and have vertically constant transport below the surface layer. The indirectly wind-forced circulation \mathbf{u}_{wi} gives rise to a two-cell overturning structure which opposes the directly forced circulation. This response can be interpreted as the result of a downward advection of isopycnal surfaces in the thermocline. The thermocline depth (defined as the depth of maximum averaged upwelling over the southern half of the domain) is increased by wind forcing from 0.19 of the full depth, in run S0R0, to 0.24 in run S0WR0. This increases the penetration of the surface forcing, leading to increased zonal overturning and hence more meridional overturning in the north.

In the southern part of the subtropical gyre region \mathbf{u}_{wi} has a negative overturning cell which is associated with the horizontal circulation of \mathbf{u}_w ; the wind-driven subtropical gyre circulation increases the strength of the western boundary current and the southward flow at the eastern boundary, warming and cooling the western and eastern boundaries respectively. This reverses the eastward density gradient near to the southern boundary and leads, by geostrophy, to negative vertical shear in the northward velocity, and hence to negative meridional overturning. In this case the run without wind (S0R0) has a maximum value of Ψ_M of 1.85×10^{-2} (24 Sv). The purely thermally driven overturning (the zonal average of $\mathbf{u}_2 - \mathbf{u}_w$) in the run with wind (S0WR0) has a two-cell structure with extremal values of Ψ_M of 2.0×10^{-2} in the north and -4.9×10^{-3} in the south, which combine with the wind forced velocities to give a maximum value of Ψ_M of 1.93×10^{-2} ; about 5 percent larger than the maximum without wind. With variable surface salinity, the effect is complicated because the gyre circulation can partially isolate water masses leading to more extreme values of surface salinity. Below the surface, however, isosurfaces of temperature and salinity are closely related and the dominant effect of wind forcing in our temperature-dominated solutions is always a deepening of the thermocline and an increase in the maximum meridional overturning.

With bottom slope the effects of changes in wind forcing are more subtle and the increase in overturning caused by wind forcing is not accompanied by an increased resistance to the onset of oscillations. This may be because the oscillations found with slope up to the north do not involve a complete collapse of the direct overturning cell, which is merely weakened and reduced in extent during the deep warming phase. These changes in the character of the oscillations are discussed in Section 5.4.

5.3 Effect of bottom slope and wind on the period of oscillations

To determine the effect of slope and wind stress on the period of the oscillations we have integrated runs S0WR2.7, S2WR2.7 and S0R2.7 for a period of over eight thousand years. 2.7 is the minimum salinity forcing amplitude found for which runs with these slope and wind parameters all oscillate. Since these runs contain less than two complete cycles we have no proof that the oscillation periods will not change with time, nor even that the oscillations are essentially regular rather than completely chaotic. However, the behaviour of the model following the second collapse is very similar to that following the first; furthermore in another run described later which has a much shorter period,

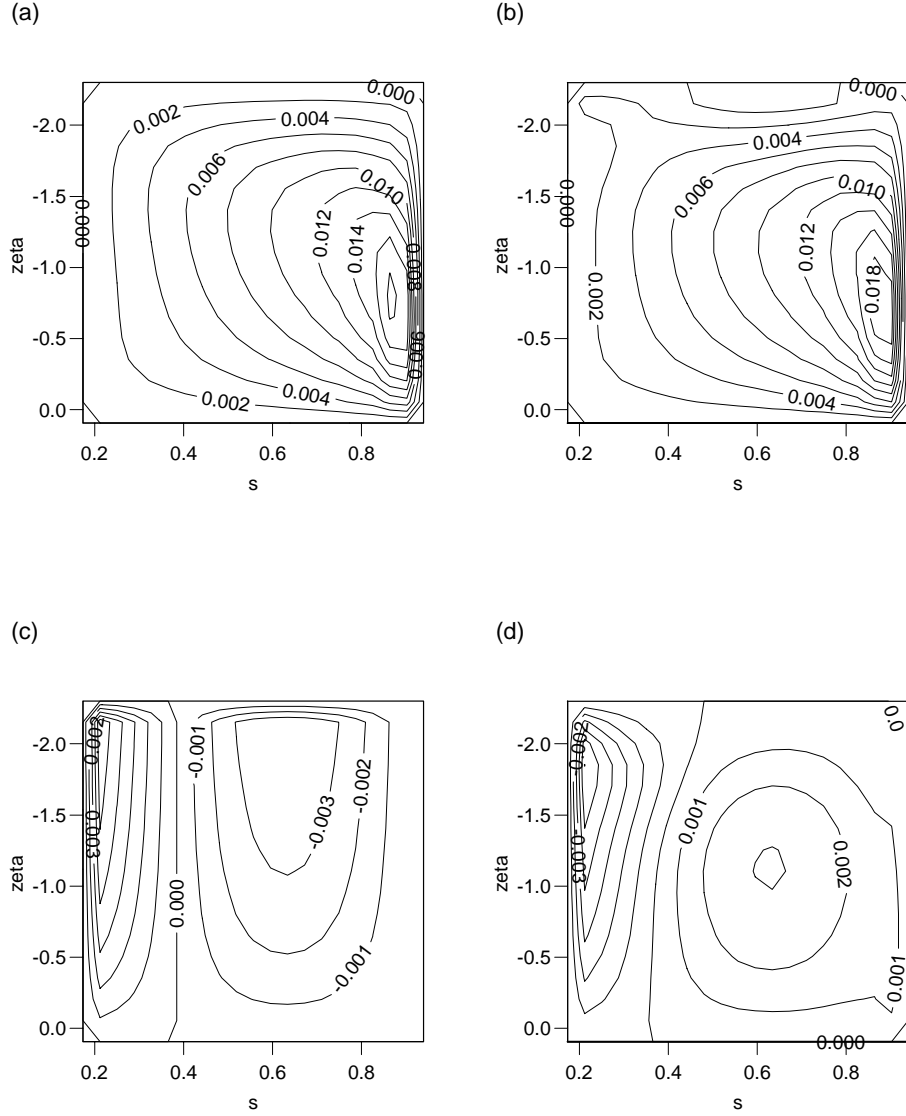


Figure 8: Zonally averaged meridional overturning fields (a) run S0R0, without wind (b) run S0WR0, with wind (c) directly wind-forced overturning in run S0WR0, the average of \mathbf{u}_w , (d) indirectly wind-forced overturning in run S0WR0, the average of \mathbf{u}_{wi} . The sum of the fields in (c) and (d) is the difference between the fields in (b) and (a). Dimensional values can be obtained by multiplying by 1274 Sv. Vertical levels are uniformly spaced in the logarithmic coordinate $\zeta = \log(1 - z + 0.1)$.

Table 2: Oscillation periods in years for the runs described in Section 5.3

run	flush phase	collapsed phase	period
S0WR2.7	760	4310	5070
S2WR2.7	100	3470	3570
S0R2.7	420	4350	4770

the oscillation period was found to change very little during 7 complete cycles. Winton and Sarachik (1993) exhibit several complete cycles from a range of runs using different salinity forcing, of which only the run with the largest forcing amplitude clearly shows irregular behaviour. We define the period as the time between the first and second minima in the record of average deep temperature.

Time series of average deep temperature for the three cases are shown in Figure 5. The periods are given in Table 2. Upslope leads to a significant reduction in period, while removing the wind stress also reduces the period. Conditions which favour the onset of oscillations therefore also result in oscillations of shorter period in these cases.

This trend is most evident in the lengths of the cooling flush phases. The destabilizing effect of slope in run S2WR2.7 results in the shortest cooling phase. Since the rate of change of average deep temperature behaves similarly in all three cases, the shorter cooling phase results in a higher average deep temperature at the start of the warming phase. Consequently the warming phase is also shortest in run S2WR2.7 and hence the overall period is the shortest of the three experiments. The stabilizing effect of wind is apparent in the increased cooling time in run S0WR2.7, as compared to run S0R2.7. The longer cooling phase results in a slightly lower average deep temperature at the start of the warming phase, but the warming phase also ends at a lower temperature in the wind driven run, so the length of the warming phase is actually marginally shorter with wind.

The presence of bottom slope has only a very small effect on the meridional overturning streamfunction in the collapsed phase. Without wind there is a single, southern-sinking cell, the strength of which varies by less than 20 percent during the collapsed phase. With wind there is also a direct cell in the south so that sinking occurs on average in mid-latitudes. The direct cell deepens and increases in strength by about 70 percent during the collapsed phase. Figure 9 shows the meridional overturning streamfunction Ψ_M near the end of the collapsed phase in runs S0WR2.7, S2WR2.7 and S0R2.7. The extra wind driven circulation affects the advection of warm water to the deep and is therefore partly responsible for the small change in the rate of deep warming.

In conclusion it appears that for these three runs the conditions which were shown above to favour the thermally driven circulation also result in a longer flush phase and hence a longer oscillation period. However this simple trend is not maintained for all values of salinity forcing as we will see in the next section, where the reason for the higher maximum deep temperature and hence the slightly longer collapsed phase without wind becomes apparent.

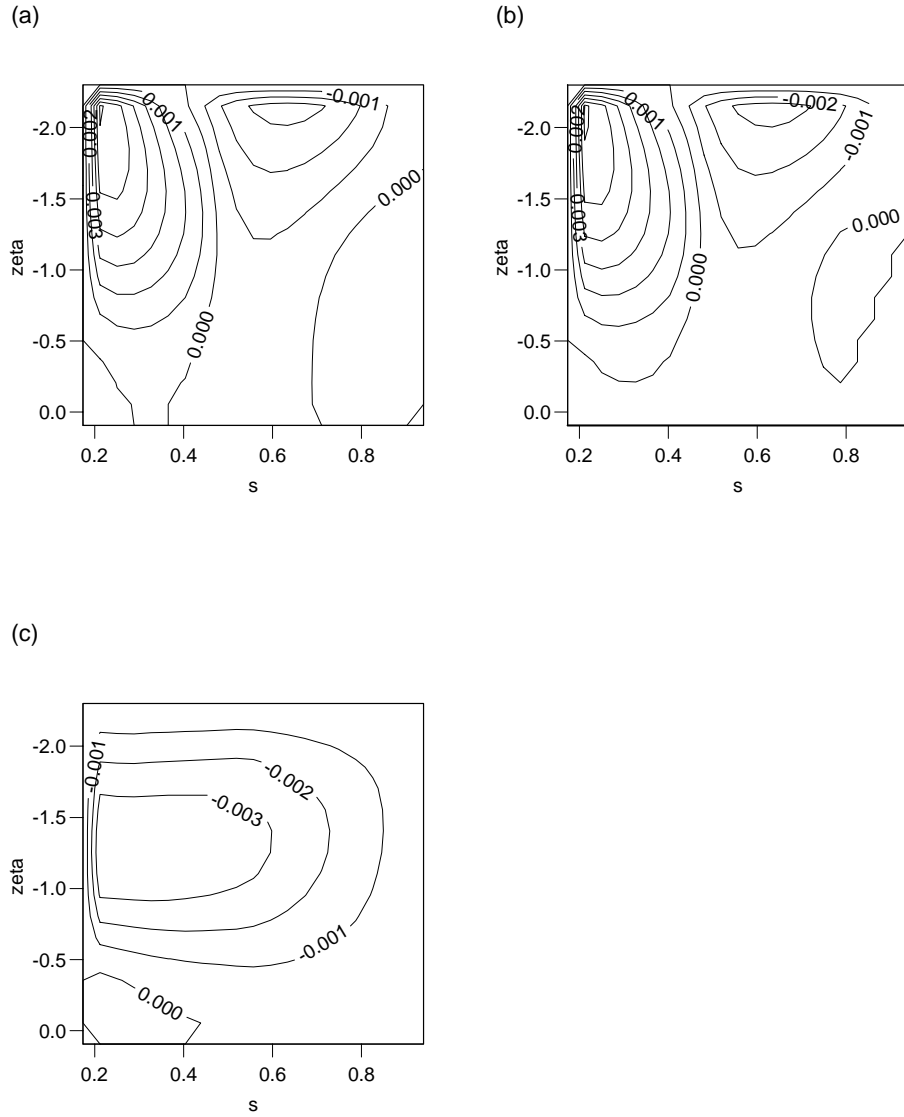


Figure 9: The meridional overturning streamfunction near the end of the collapsed phase for runs S0WR2.7, with wind (a); S2WR2.7, with wind and slope (b); and S0R2.7, without wind or slope (c). Dimensional values can be obtained by multiplying by 1274 Sv. Vertical levels are uniformly spaced in the logarithmic coordinate $\zeta = \log(1 - z + 0.1)$

5.4 Effect of salinity forcing on the oscillation period

With a bottom slope parameter of +2, oscillations occur at a smaller salinity forcing, so we can consider how a reduction in salinity forcing affects the oscillations. Runs S2WR2 and S2R2 both oscillate, but with radically different periods of 1135 years and 5026 years respectively. The effect of wind stress on the oscillation period has therefore been drastically enhanced with an upslope and reduced salinity forcing, and is opposite to that found above. This is because the higher average deep temperature maximum noted above in the case without wind has become the dominant factor determining the length of the collapsed phase, and hence the overall period. With wind, in run S2WR2, the deep temperature ranges from 8 to 15 whereas in run S2R2 the range is from 8 to 19. The result is a much shorter oscillation in the case with wind.

To understand this it is necessary to investigate how the collapsed phase ends. The end is marked by a sudden increase of convection in the north, leading to a powerful thermally driven overturning state with sinking in the north. Convection in the north brings warmer water up from the deep, enhancing the convection and the northern sinking by increasing the surface heat loss. Because of this feedback, localized deep convection in the north could accelerate the process of destabilization over a wider area. Density sections shown in figures 10 and 11 show that the flushes in runs S2WR2 and S2R2 are initiated when convection first reaches from the surface to the bottom of the domain. Western boundary sections are plotted, eastern boundary sections are essentially the same.

This situation triggers a rapid flush but it does not occur until much slower diffusion-driven density changes have rendered the fluid neutrally stable over the entire depth of a vertical column. In run S2WR2 this occurs at the northern wall where the domain is shallowest, at a time when the deep ocean is still stably stratified. Without wind in run S2R2 the northern halocline region remains stably stratified and the flush is not initiated until much later, when the static stability of the deep water south of the slope region has been eroded. Immediately before the flush in run S2R2 examination of terms in the dynamic equations shows that temperature is a stabilizing influence at the northern wall while salinity is destabilizing. Figure 12 shows the vertical variation of terms in the salinity equation at the centre of the northern wall shortly before the flush for the two runs. The horizontal and vertical components of advection are defined as $\mathbf{u}_h \cdot \nabla S$ and $w \partial S / \partial z$, where h denotes the horizontal, rather than $\nabla_h \cdot (\mathbf{u} S)$ and $\partial(wS) / \partial z$ as calculated in the model. Notice that the horizontal advection (HA) term is mostly positive in run S2WR2 and negative in run S2R2. Although it is not the largest term the change in horizontal advection is more than enough to account for the change in $\partial S / \partial t$ between the two cases and the consequent changes in stability. A similar pattern exists all along the northern wall. Away from the wall horizontal salinity advection in run S2WR2 becomes more important relative to the other terms as shown in figure 13.

The horizontal salinity advection in run S2WR2 is due to a strong northward barotropic flow over the slope. Removing the directly wind-forced part of the velocity approximately halves the value of HA at the northern wall and reverses the destabilizing trend, but still leaves a strong northward barotropic flow driven by slope effects (JEBAR). Even the baroclinic component of the flow contributes to the destabilization by HA of

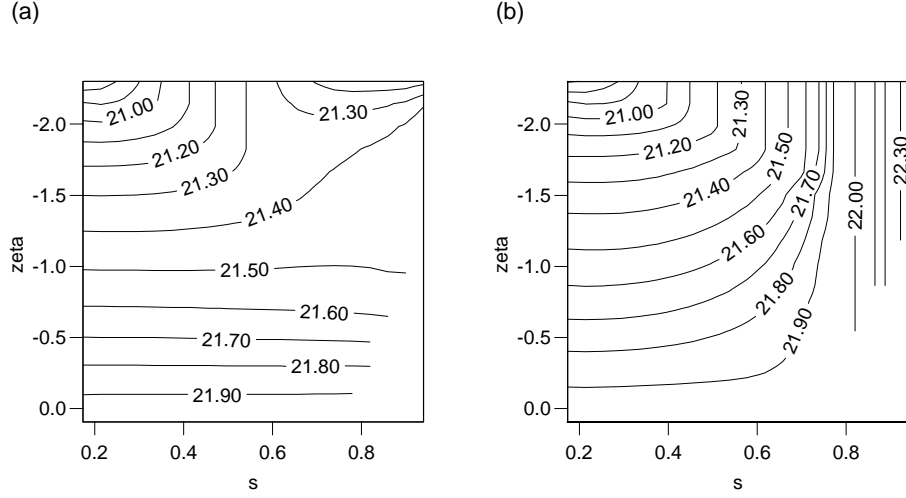


Figure 10: Density sections at the western boundary at approximately (a) 4; (b) 0 years before the flush in run S2WR2 with wind and slope. Vertical levels are uniformly spaced in the logarithmic coordinate $\zeta = \log(1 - z + 0.1)$. The northward coordinate is sine latitude.

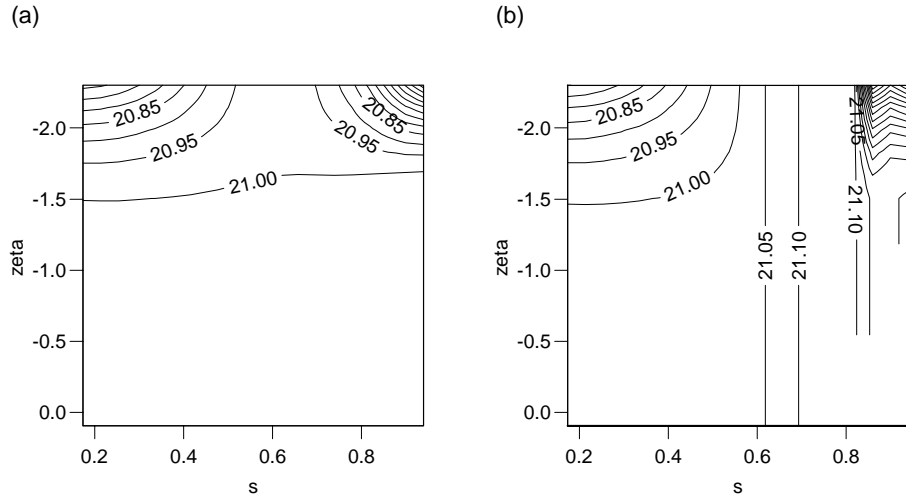


Figure 11: Density sections at the western boundary at approximately (a) 4; (b) 0 years before the flush in run S2R2 without wind. Vertical levels are uniformly spaced in the logarithmic coordinate $\zeta = \log(1 - z + 0.1)$. The northward coordinate is sine latitude.

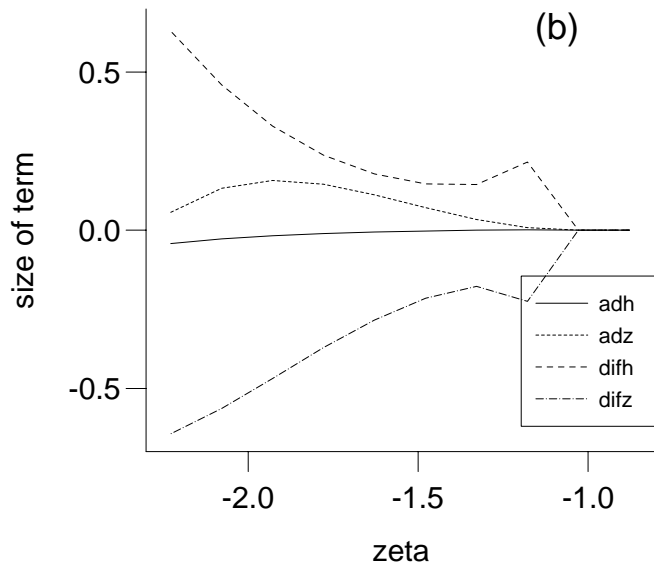
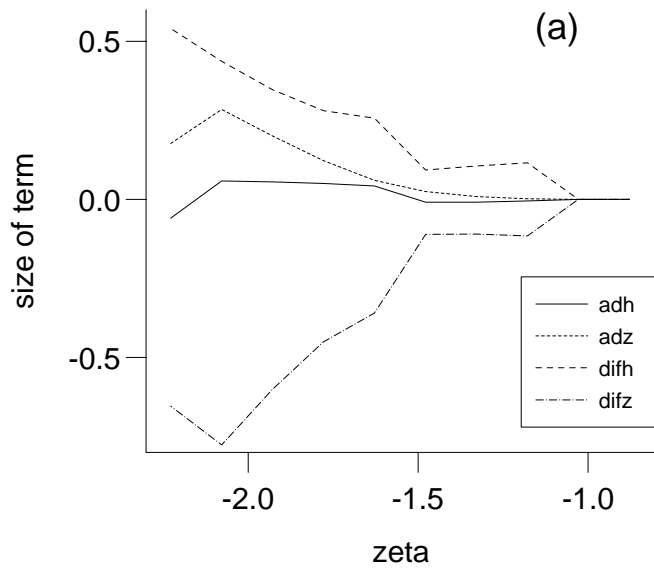


Figure 12: Vertical variation of terms in the salinity equation for runs S2WR2 with wind (a) and S2R2 without wind (b) at the centre of the northern wall shortly before the onset of a flush.

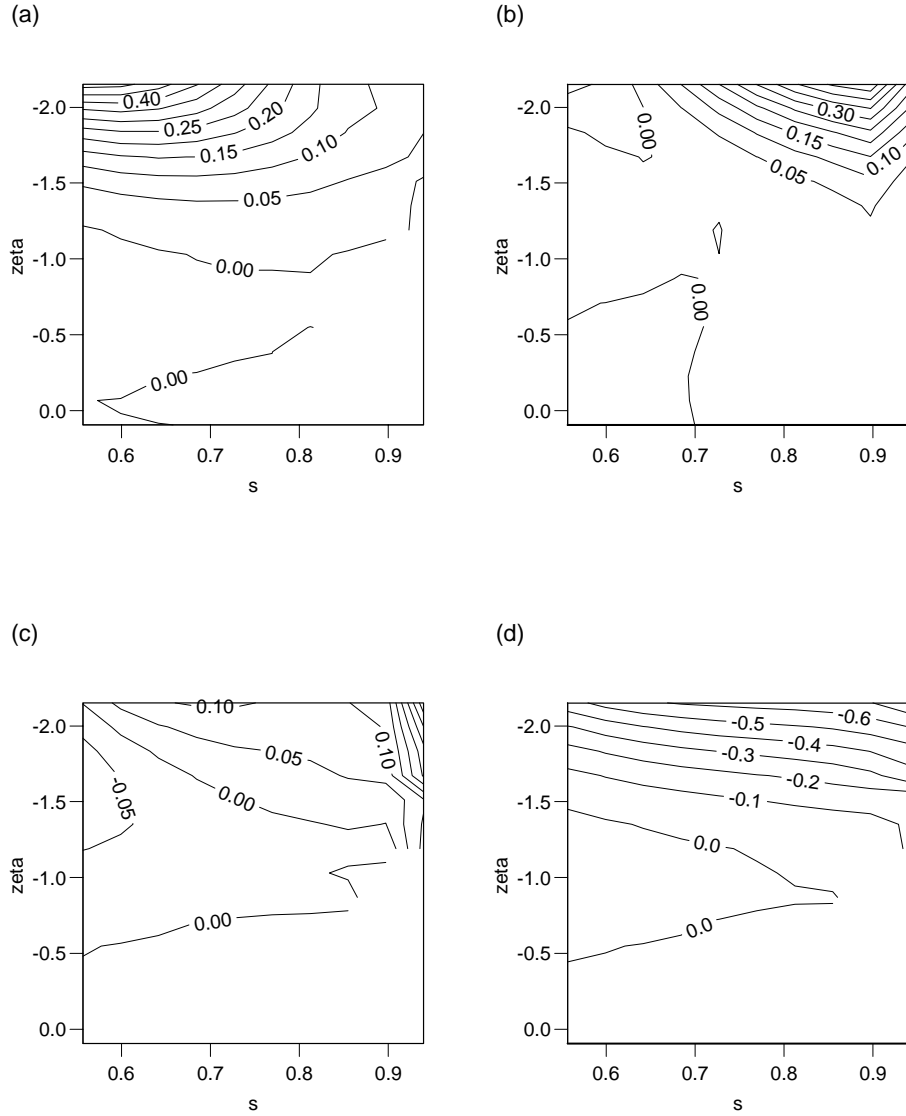


Figure 13: Vertical and northward variation of terms in the salinity equation for run S2WR2 at mid-basin in the northern half of the domain shortly before the flush. The surface layer, in which the principal balance is between vertical diffusion and horizontal advection, is not shown. (a) horizontal advection, (b) vertical advection, (c) horizontal diffusion, (d) vertical diffusion. Vertical levels are uniformly spaced in the logarithmic coordinate $\zeta = \log(1-z+0.1)$. The northward coordinate is sine latitude.

salinity, although the baroclinic component of the flow at the northern wall is an order of magnitude smaller than the barotropic component. Immediately before the flush in run S2R2 the meridional velocity over the slope is weaker in magnitude and takes the opposite sign to that in S2WR2.

The velocity differences between the two runs in the collapsed phase are related to radically different density structures. In run S2R2 the density structure is dominated by a northern halocline with stability decreasing to the south. The corresponding zonally averaged meridional overturning shows a single, southern sinking cell. With wind, in the collapsed phase of run S2WR2, there is a strong southern thermocline structure with isopycnal surfaces rising northwards while the northern halocline structure is restricted to the north east corner of the domain. The resulting flow is strongly trapped in the upper ocean, but the main meridional overturning cell reflects the thermal driving, with sinking towards the north. A weaker reversed cell is confined above and to the north of the main cell. The thermally driven character of the flow in the west and north in run S2WR2 leads to a JEBAR-driven barotropic flow which reinforces the subpolar wind gyre, as in the simulation described in Section 4, while the density gradients and hence the barotropic flow in run S2R2 are in the opposite sense during the collapsed phase. In fact the barotropic flow in run S2WR2 is deceptive, for the strength of the subpolar gyre is similar to the value with a flat bottom, but is dominated by the JEBAR effect. The directly wind-forced contribution is five times smaller over this slope for the same wind stress because of the resistance to moving up the slope, related to vertical stretching and large changes of potential vorticity.

If the salinity forcing is again reduced, this time to the minimum found for oscillatory solutions, the period decreases drastically with or without wind forcing, but remains shorter with wind stress than without. Run S2WR1.7 has a period of 654 years and run S2R1.7 has a period of 2343 years. At this smaller value of salinity forcing, neither of the runs has completely reversed circulation in the collapsed phase, which in both runs resembles run S2WR2: there is a two-cell structure with the salinity-driven, reversed cell trapped in the north. However without wind in run S2R1.7 the density structure in the north in the collapsed phase is more uniform zonally than in run S2WR1.7 and the flush is again initiated by deep convection at mid-latitudes, while the deep convection immediately before the flush in run S2WR1.7 occurs at the north. Re-examination of the flat bottomed oscillating runs S0WR2.7 and S0R2.7 shows that the location of the initial deep convection before a flush shows the same pattern; at the north with wind and at mid-latitudes without.

Note that with slope parameter +2, varying the salinity and wind forcing gives oscillations which range in period by a factor around eight. Without topography in our model, we have only found very long period oscillations with the forcing and dissipation parametrizations chosen. With slope the period increases with salinity forcing, but not indefinitely; with the salinity forcing increased to a relative value of 4 in run S2WR4 we find the period has reduced to 2300 years, as a result of stronger reversed overturning and more rapid deep warming. The period of the flat bottom runs also decreases for stronger salinity forcing. For run S0WR4 the period is 2900 years, decreasing further to 2000 years in run S0WR6.

In conclusion it transpires that wind forcing can promote destabilization by salinity

Table 3: Average overturning in steady solutions

run	Ψ_Z max	Ψ_M max
S2WR1	0.91×10^{-2}	1.25×10^{-2}
S0WR1	1.79×10^{-2}	1.65×10^{-2}
S-1WR1	1.83×10^{-2}	2.16×10^{-2}

advection towards the northern wall, prematurely ending the collapsed phase and reducing the oscillation period. For the flat bottom run S0WR2.7 this effect is too small to counteract the longer flush time, so the overall period is still longer than in run S0R2.7, but with slope parameter +2 the result is a radical reduction in period for the runs with wind. The deep convection which ends the collapsed phase always occurs first at the northern wall when there is wind forcing. Without wind forcing the initial destabilization occurs in mid-latitudes, in between the warmer subtropical water and the fresher subpolar water. With upslope a reduction in salinity forcing produces much smaller amplitude oscillations in which the flow in the deep warming phase, although weak in the deep and lacking strong northern convection, is not salinity dominated except in a small region, and the oscillation period is much shorter. The period of these smaller amplitude oscillations increases with salinity forcing, up to a relative salinity forcing of around 2.7. Further increasing the salinity forcing leads to a decrease in period, with or without slope. This decrease occurs for two reasons: firstly the shorter flush phase results in warmer deep water at the start of the collapsed phase; and secondly stronger reversed overturning in the salinity-driven phase increases the rate of deep warming by advection and convection in the south. Hence we expect there to be a maximum period for these oscillations, probably determined by the rate of heat diffusion from the surface to the deep ocean. We investigate this possibility below.

6 Solutions with other geometries and dynamics

We now discuss solutions with downslope to the north, solutions with slope to the east and west, and solutions using dynamically reduced versions of the model. These simulations may have less direct relevance to the ocean, but are intended to improve understanding of the effects of topography and of the behaviour of our model in general.

6.1 Solutions with downslope

We now consider solutions with slope parameter equal to -1 to see whether the explanations of slope effects put forward so far are robust. Figure 14 shows the barotropic streamfunction for run S-1WR1. The JEBAR forcing term in this run opposes and overrides the wind stress, leading to a strong anticyclonic gyre in the north. The maxima of Ψ_Z and Ψ_M are both greater than in the flat bottom case, consistent with the trend already found, see Table 3. The increased overturning suggests that the solution should be more stable to the onset of oscillations. This turns out not to be the case

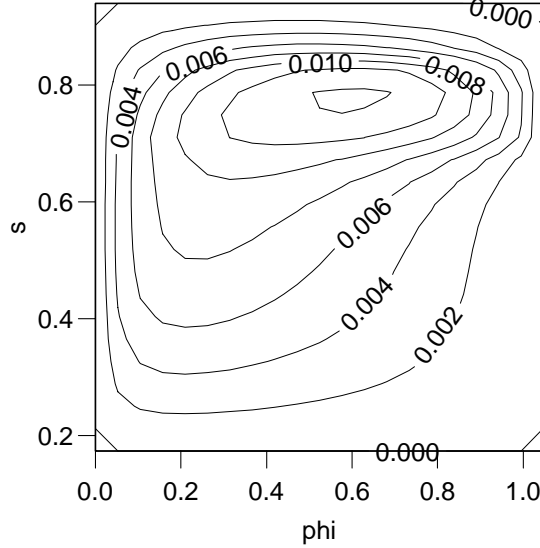


Figure 14: Barotropic streamfunction for run S-1WR1 with downslope to the north. Dimensional values can be obtained by multiplying by 1274 Sv. The northward coordinate is sine latitude.

although the difference in the stability boundary between flat and downslope runs is very small. With wind the boundary occurs between runs S-1WR2.5 and S-1WR2.6 and without wind between runs S-1R2.3 and S-1R2.4. Thus the difference in stability has not been resolved by our experiments without wind but with wind the downslope appears marginally less stable than the flat bottom.

One reason that the downslope has less effect on stability than the upslope may be the uniformity of the deep temperature and salinity. The downslope effectively introduces a trench filled with more deep water of the same properties, whereas the deepest water over the upslope has significantly different characteristics. Comparing runs S0WR2.6 (which becomes steady) and S-1WR2.6 (in which the flow collapses) the reduced stability in the downslope run appears to be caused by strong horizontal salinity advection by the barotropic flow. This decreases the static stability of the downslope run in the north west but increases it in the north east convecting region. This ultimately leads to a breakdown of convection there and a collapse of the circulation, even though the meridional overturning remains stronger with the downslope until the collapse occurs.

Run S-1WR2.7 was found to have an oscillation period of 6000 years, much longer than either the flat or upslope runs at the same salinity forcing. Since the range of deep temperature during the decoupled phase was similar to the other runs, this is likely to be due to the increased time taken for heat to diffuse to the deep water. Note that the diffusion timescale H^2/κ_V takes a value around 2700 years in the flat bottom case, within a factor of around two of the longest oscillation periods found. The maximum depth in the downslope run is 1.5 times greater, hence an estimate based on the maximum depth alone gives a diffusion timescale twice as long for the downslope run. Below we consider

run	max Ψ_M	max Ψ_ρ	max Ψ_Z	min Ψ	max Ψ
ES2WR1	1.7×10^{-2}	1.4×10^{-2}	1.1×10^{-2}	-1×10^{-2}	6×10^{-3}
WS2WR1	1.9×10^{-2}	1.7×10^{-2}	1.6×10^{-2}	-2×10^{-3}	2×10^{-2}
S2WR1	1.3×10^{-2}	1.5×10^{-2}	9.1×10^{-3}	-2×10^{-2}	4×10^{-3}
S0WR1	1.7×10^{-2}	1.6×10^{-2}	1.8×10^{-2}	-3×10^{-3}	5×10^{-3}

Table 4: Mean values for runs with eastern and western slope

further whether diffusion can provide an upper bound for the oscillation timescale.

6.2 Eastern and western slope

Two steady solutions have been derived with slope up towards the eastern and western boundaries analogous to the northern slope with parameter +2. Standard forcing amplitudes were used so the runs are denoted ES2WR1 and WS2WR1 respectively. Both runs were broadly similar to the basic solution of Section 3 with deep sinking in the north, and convection reaching the deepest water in the domain at the northern wall. The northward increase of density results in topographically forced barotropic gyres which, in both cases, promote northward barotropic flow along the slope. Since the return flow can occupy the full depth of the domain, this recirculation contributes to Ψ_M , which is consequently a less appropriate indicator of the stability of the circulation in these runs. Ψ_M is in both cases larger than it is in the flat bottomed run S0WR1, but in contrast to the northward shallowing runs, the trend in Ψ_M is not matched by similar trends in Ψ_Z , convective frequency, and the integrated surface heat loss. Döös and Webb (1994) describe how in steady flows an alternative zonally averaged meridional overturning streamfunction Ψ_ρ can be defined which measures the amount of fluid which crosses density surfaces.

$$\Psi_\rho(s, \rho) = \int_{\phi_W}^{\phi_E} \int_{\rho_{max}}^{\rho} v \cos(\theta) dz d\phi \quad (17)$$

where ϕ_W and ϕ_E are the longitudinal limits of the domain, θ is latitude and ρ_{max} is the maximum value of density. The difference between Ψ_M and Ψ_ρ depends on how closely coincident are surfaces of constant height, density and northward velocity. Ψ_M is generally more appropriate for the simple dynamics and geometry of our model, but for these two runs the topography may make Ψ_ρ more relevant. Values are given in Table 4.

We have also found the stability boundary for these geometries, as in Section 5. The eastern slope did not affect the bifurcation point, which occurred at a relative salinity forcing amplitude of around 2.7. The western slope configuration, on the other hand, was significantly less stable, bifurcating at a forcing amplitude of around 2.3. Processes occurring close to the western boundary are therefore very important to the stability of the thermally driven circulation. This is no surprise as the constraint of Sverdrup vorticity balance in the interior means that the western boundary current dominates the

northward heat transport and overturning. There is also strong upwelling at the western boundary in our solutions, and convection in the basic solution, although stronger in the north east, is deeper in the north west.

6.3 Pure diffusion solutions

By neglecting all advection and convection we arrive at a system consisting of two simple, decoupled diffusion problems for heat and salt. The steady diffusive problem was discussed by Wright and Stocker (1991) who suggested that it was relevant to the evolution of the temperature and salinity in the deep ocean during the collapsed phase of deep decoupling oscillations. There is very little advection in the deep during the collapsed phase and they proposed that the deep temperature and salinity would evolve towards the solution of the pure diffusion problem. They showed that the steady solution to the pure diffusion problem could not be statically stable everywhere in the deep with their choice of forcing and linked this fact to the convective flush which ultimately ends the collapsed phase. This raises some interesting points. If the equation of state is linear, and the patterns of surface temperature and salinity happen to be proportional, then there is a precise value of forcing in which the contributions of temperature and salinity to the density exactly cancel and the steady solution is everywhere exactly neutrally stable. For any other value of forcing, or if the surface forcing functions for S and T are not precisely proportional, then there must indeed be static instability somewhere in the steady solution if we retain the assumption of a linear state equation.

To see this, note that S and T and hence density ρ all obey Laplace's equation in the interior, hence by the divergence theorem the integral of the normal derivative over the boundary of the domain must be zero. With insulating walls this means that the integral of $\partial\rho/\partial z$ over the surface boundary at $z = 1$ must be zero. The same applies to the integral over any interior surface $z = \text{constant}$ within the domain, thus there are only two possibilities; either the solution is everywhere exactly neutral, which is the case noted above, or else instability must occur somewhere in the domain. It is not possible for the solution to be non-trivially stable anywhere without also being unstable somewhere else. This is purely a result of the divergence theorem and boundary conditions and is independent of the shape of the domain. However with a nonlinear equation of state the result no longer holds. The dominant nonlinearity in our equation of state is a quadratic contribution to the thermal expansion which increases the thermal expansivity with temperature. This raises the possibility of non-trivial steady diffusive solutions which are statically stable everywhere. The stabilizing effect of salinity forcing in the north can outweigh the destabilizing effect of temperature there, while in the warmer south the nonlinearity might allow temperature to have the greatest effect on density and maintain stability there also. We were interested to question at what value of forcing (if any) such solutions might exist for the forcing patterns used in the present model and also what would be the result of initializing the fully advective model with such a diffusive solution.

Advective effects are of leading order in the thermally driven mode throughout most of the domain unless the surface forcing is reduced by a factor of order 100 (Colin de Verdière 1988). Hence the relevance of the pure diffusion solutions is severely restricted

except possibly during the collapsed phase of the deep decoupling oscillations. The extremely long timescale for these oscillations is an indication that their period may indeed be strongly influenced by diffusion. We investigate this possibility below.

In principle time-dependent solutions to the pure diffusion problem could be derived analytically, for instance by transform methods, but we have opted instead to solve the problem numerically to make the correspondence between the full and reduced models as straightforward as possible. Using exactly the same grid and numerical parameters as before, the diffusive problem (which is only two-dimensional) can be integrated until the solution converges exactly.

Example steady solutions are shown in figure 15. Steady solutions for T and S at different amplitudes of surface forcing are simply linear combinations of the solutions for T and S at a standard forcing amplitude. By diagnosing the resulting density we can find the amplitude of salinity forcing which results in the minimum amount of static instability in the steady solution. Because of the lower boundary condition the stratification always approaches neutrality close to the bottom. This results in a small finite amount of instability near the bottom except very close to a certain amplitude of salinity forcing which is approximately 1.95 for slope parameter 0 or +2. In contrast to the behaviour with a linear equation of state the fluid above is stably stratified at around this value of forcing with an average top to bottom density difference of about 0.15.

There is no evidence that this represents a special value of forcing for the model with full dynamics. If the full model is initialized with a state which represents a steady solution to the pure diffusion problem and is statically stable everywhere, then a weak, surface-trapped circulation is set up which eventually results in a flush. That is, the deep decoupling oscillation behaviour previously found close to this value of forcing continues irrespective of the initial condition. Steady solutions of the full model typically occur at values of surface forcing which produce regions of strong static instability in steady solutions with only diffusion.

We wish to know whether the length of the collapsed phase is governed by diffusion. In particular, does the time taken for instability to appear in the pure diffusion solutions provide an upper bound on the length of the collapsed phase? To answer this question we initialize the pure diffusion model with the zonal average of the state derived from the full model at the start of the collapsed phase, shortly after the end of the flush phase, and measure the time taken for instability to appear in the lower half of the physical domain ($z < 0.5$). The results given in Table 5 are consistent with the conjecture that the pure diffusion solution provides an upper bound for the length of the collapsed phase and hence the period. The time to instability in the pure diffusion solution increases with the average depth of the domain and also increases near to the forcing amplitude at which the diffusive solution is stable everywhere. Significantly shorter periods were found in the full model when a premature collapse occurred before the deep water had become unstable.

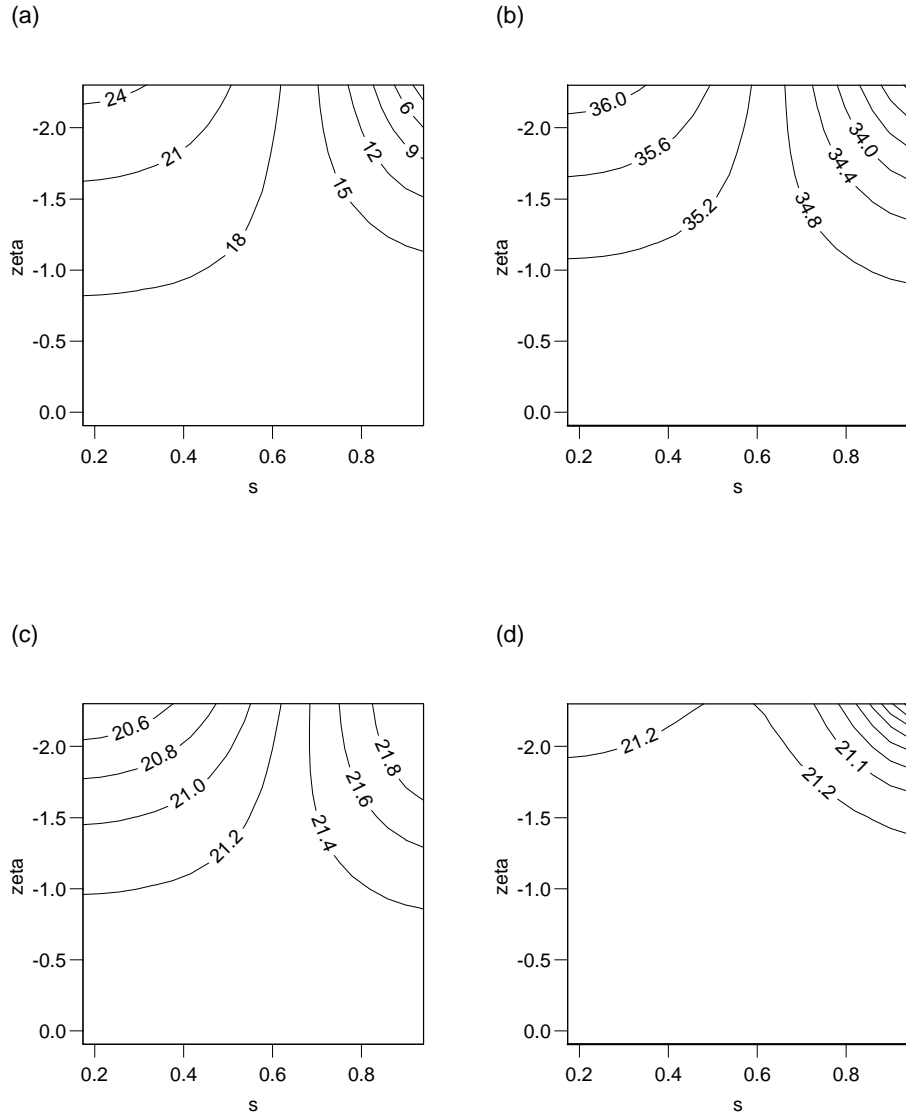


Figure 15: Steady pure diffusion solutions; (a) T , (b) S , and (c) ρ for run S0R1, and (d) ρ for run S2R1.95. Vertical levels are uniformly spaced in the logarithmic coordinate $\zeta = \log(1 - z + 0.1)$. The northward coordinate is sine latitude.

run	time to instability (years)	oscillation period (years)
S0WR2.7	3717	5070
S0R2.7	3636	4767
S2WR2.7	3070	3575
S2WR2	5898	1135
S2R2	5818	5026
S2WR1.7	4121	654
S2R1.7	4202	2343
S-1WR2.7	6383	6011

Table 5: Time to instability in pure diffusion solution

7 Conclusions

We have used a frictional geostrophic ocean circulation model to examine the stability of the thermohaline circulation to oscillations during which the overturning collapses. This study has focused on the destabilizing effects of simple, idealized topographic variations and the presence or absence of wind stress.

A large scale slope up towards the north can significantly destabilize the circulation. This is partly because the efficiency of northern convection is reduced, and partly the result of topographically induced changes to the barotropic flow. A slope up towards the west also destabilizes the flow, while a slope to the east does not, indicating that the deep sinking region in the north west is critical in maintaining northern sinking in this type of model. Making the domain deeper towards the north had a smaller effect on stability because of the homogeneity of the deep water.

Wind stress can stabilize the circulation by deepening the thermocline in the subtropical gyre. Wind driving also affects the nature of oscillations and, in a certain forcing regime, wind-induced salinity advection can radically reduce the length of the collapsed phase, by destabilizing the northern halocline. Without wind, the collapsed phase ends when deep convection starts in mid-latitudes.

Unless unreasonably strong salinity forcing is used the deep currents in the collapsed phase are weak, and the overall period of the oscillation is usually governed by the time taken for diffusive warming to destabilize the deep. Stronger overturning in the direct, thermally driven phase can increase the stability of the deep water at the start of the collapsed phase and hence increase the overall period. The shortest oscillation periods of a few hundred years were found for weak salinity forcing with slope up to the north, when the thermally driven overturning only partially collapsed.

The pure diffusion problem is relevant to the deep water in the collapsed phase. With a linear equation of state, non-trivial steady solutions to this problem are always statically unstable in some region. With a nonlinear equation of state, solutions to the pure diffusion problem exist which are statically stable everywhere, except possibly close to the bottom. Nonlinearity in the equation of state also affects the solutions with full

dynamics; if the nonlinearities are neglected, salinity-dominated solutions with strong sinking near the equator and upwelling near the pole can be found which are steady. With a nonlinear equation of state, such solutions are always unsteady within the range of forcing considered. Winton (1993) has shown that nonlinearities in the equation of state can enhance thermocline variability.

Although the effects of ocean atmosphere exchange on thermohaline stability have been studied by Zhang *et al.* (1993) and others (see Section 1), the interaction which we have observed between wind and topographic effects suggests that a full understanding of such a nonlinear problem would require these effects to be modelled together, as well as in isolation. The powerful surface fluxes of heat and salt which occur in subpolar regions during these oscillations would certainly be modified by more accurate models of ocean-atmosphere-sea ice interaction, possibly revealing complicated behaviour. Another potentially important extension to the current model would be to include other ocean basins, particularly as such a system could support a wider variety of modes of circulation.

Acknowledgement. This work was supported by U.K. Natural Environment Research Council Grant GR3/8578.

REFERENCES

- Adcroft, A., C. Hill and J. Marshall, 1996: Representation of topography by shaved cells in a height coordinate ocean model. Submitted to *Monthly Weather Review*.
- Bryan, F., 1986: High-latitude salinity effects and interhemispheric thermohaline circulations. *Nature*, **323**, 301–304.
- Colin de Verdière, A., 1988: Buoyancy driven planetary flows. *J. Mar. Res.*, **46**, 215–265.
- Colin de Verdière, A., 1989: On the interaction of wind and buoyancy driven gyres. *J. Mar. Res.*, **47**, 595–633.
- Darby, M. S. and A. J. Willmott, 1997: A numerical model for interdecadal variability of sea ice cover in the Greenland-Norwegian Sea. submitted to *Climate Dynamics*
- Döös, K. and D. J. Webb, 1994: The Deacon cell and other meridional cells of the southern ocean. *J. Phys. Oceanogr.*, **24**, 429–442.
- Edwards, N. R., 1996: Unsteady similarity solutions and oscillating ocean gyres. *J. Mar. Res.*, **54**, 793–826.
- Gill, A. E., 1982: *Atmosphere-ocean dynamics*. Academic Press, 662 pp.
- Killworth, P. D., 1989: On the parameterization of deep convection in ocean models. *Parameterization of small scale processes*, P. Muller and D. Henderson, Eds., Hawaii Institute of Geophysics special publication, University of Hawaii, 55–74.
- Lenderinck, G. and R. J. Haarsma, 1996: Modelling convective transitions in the presence of sea ice. *J. Phys. Oceanogr.*, **26**, 1488–1467.
- Lenderinck, G. and R. J. Haarsma, 1994: Variability and multiple equilibria of the thermohaline circulation associated with deep water formation. *J. Phys. Oceanogr.*, **24**, 1480–1493.

- Marshall, D., 1996: How slippery are piecewise-constant coastlines in numerical ocean models? submitted to *Tellus*.
- Mikolajewicz, U. and E. Maier-Reimer, 1990: Internal secular variability in an ocean general circulation model. *Climate Dyn.*, **4**, 145–156.
- Pierce, D. W., K. Y. Kim and T. P. Barnett, 1996: Variability of the thermohaline circulation in an ocean general circulation model coupled to an atmospheric energy balance model. *J. Phys. Oceanogr.*, **26**, 725–738.
- Rahmstorf, S., 1993: A fast and complete convection scheme for ocean models. *Ocean Modelling*, **101**, (unpublished manuscript)
- Rahmstorf, S., 1996: Comments on “Instability of the thermohaline circulation with respect to mixed boundary conditions: is it really a problem for realistic models?” *J. Phys. Oceanogr.*, **26**, 1099–1105.
- Rahmstorf, S., 1995: Bifurcations of the Atlantic thermohaline circulation in response to changes in the hydrological cycle. *Nature*, **378**, 145–149.
- Rahmstorf, S. and J. Willebrand, 1995: The role of temperature feedback in stabilizing the thermohaline circulation. *J. Phys. Oceanogr.*, **25**, 787–805.
- Salmon, R., 1990: The thermocline as an “internal boundary layer”. *J. Mar. Res.*, **48**, 437–469.
- Slørdal, L. H. and J. F. Weber, 1996: Adjustment to JEBAR forcing in a rotating ocean. *J. Phys. Oceanogr.*, **26**, 657–670.
- Tziperman, E., J. R. Toggweiler, Y. Feliks and K. Bryan, 1994: Instability of the thermohaline circulation with respect to mixed boundary conditions: is it really a problem for realistic models? *J. Phys. Oceanogr.*, **24**, 217–232.
- Weaver, A. J. and E. S. Sarachik, 1991: Evidence for decadal variability in an ocean general circulation model: an advective mechanism. *Atmos. Ocean*, **29**, 197–231.
- Weaver, A. J., J. Marotzke, P. F. Cummins and E. S. Sarachik, 1993: Stability and variability of the thermohaline circulation. *J. Phys. Oceanogr.*, **23**, 39–60.
- Winton, M., 1993: Deep decoupling oscillations of the oceanic thermohaline circulation. *Ice in the climate system, Proc., NATO ASI ser.*, W. R. Peltier, Ed., Springer-Verlag, 417–432.
- Winton, M. and E. Sarachik, 1993: Thermohaline oscillations induced by strong steady salinity forcing of ocean general circulation models. *J. Phys. Oceanogr.*, **23**, 1389–1410.
- Wright, D. G. and T. F. Stocker, 1991: A zonally averaged ocean model for the thermohaline circulation. 1. Model development and flow dynamics. *J. Phys. Oceanogr.*, **21**, 1713–1724.
- Yin, F. L. and E. S. Sarachik, 1995: Interdecadal thermohaline oscillations in a sector ocean general circulation model: advective and convective processes. *J. Phys. Oceanogr.*, **25**, 2465–2484.

- Zhang, S., R. J. Greatbach and C. A. Lin, 1993: A reexamination of the polar halocline catastrophe and implications for coupled ocean-atmosphere modeling. *J. Phys. Oceanogr.*, **23**, 287–299.
- Zhang, S., C. A. Lin and R. J. Greatbach, 1995: A decadal oscillation due to the coupling between an ocean model and a thermodynamic sea-ice model. *J. Mar. Res.*, **53**, 79–106.
- Zhang, S., C. A. Lin and R. J. Greatbach, 1992: A thermocline model for ocean-climate studies. *J. Mar. Res.*, **50**, 99–124.